Available online at www.sciencedirect.com
ScienceDirect
Journal of Cultural Heritage 8 (2007) 272–283
Journal of Cultural Heritage
http://france.elsevier.com/direct/CULHER/

Original article

# Remote hyperspectral imagery as a support to archaeological prospection

Rosa Maria Cavalli [a,*], Francesca Colosi [b,1], Angelo Palombo [c,2], Stefano Pignatti [c,2], Maurizio Poscolieri [d,3]

[a] C.N.R. Istituto Inquinamento Atmosferico Sez. L.A.R.A., Via del Fosso del Cavaliere 100, 00133 Rome, Italy
[b] C.N.R. Istituto per le Tecnologie Applicate Beni Culturali, Via Salaria Km 29, 300 C.P. 10, 00016 Monterotondo Stazione (Rome), Italy
[c] C.N.R. Istituto Metodologie Analisi Ambientali, C.da S. Loja, Zona Industriale, 85050 Tito Scalo (PZ), Italy
[d] C.N.R. Istituto di Acustica ''O. M. Corbino'' Via del Fosso del Cavaliere 100, 00133 Rome, Italy

Received 31 October 2006; accepted 15 March 2007

**Abstract**

Hyperspectral data were exploited to test their effectiveness as a tool for archaeological prospection, envisaging their potential for detecting spectral anomalies related to buried archaeological structures. For this purpose the airborne Multispectral Infrared and Visible Imaging Spectrometer images were analysed. Each single band of the entire data set and different processing technique products were interpreted to identify any tonal anomalies. Since every analysed image exhibited marks different in terms of size and intensity, two indexes were defined for assessing the potential of anomalies detection of each image. Such parameters were: the *Detection Index*, used for counting the number of pixels related in each image to marks, and the *Separability Index*, applied for measuring the tonal difference of the marks with respect to the background. These indexes were tested on two areas within the Selinunte Archaeological Park where the presence of remains, not yet excavated, was supposed by archaeologists. For the test sites any extracted anomalies were evaluated by an expert in order to determine their archaeological relevance. The comparison among the index values, derived from each single band of the spectrometer and from different image processing by-products, allowed to determine which spectral range and which processing method are the most valuable to quickly highlight the anomalies. The analysis pointed out that, where vegetation cover is dominant, the Visible near infrared is the spectral region more sensitive to variations of spectral properties related to buried structures, while, where soil cover becomes relevant, the Short-wave infrared and the Thermal-infrared regions resulted more sensitive. As far as the applied processing methods are concerned, the Spectral Angle Mapper classifier and, secondly, the Minimum Distance algorithm stressed the highest archaeological information content. The results of this work showed that the archaeological information content derived by analysing the outputs of the applied image processing techniques is more significant than the information obtained by interpreting each single band and the available historical aerial photos. As a final remark, the data processing flow chart, applied to the entire remote hyperspectral data set over Selinunte Archaeological Park, appeared encouraging for detection of anomalies related to the presence of the buried archaeological structures.


*Keywords:* Hyperspectral imagery; Visible-near infrared; Short-wave infrared; Archaeological prospection; Buried structures; Spectral anomalies; Detection index; Separability index

## 1. Research aims

Few applications of Remote Sensing (R.S.) have been, up to the present, carried out for detecting buried structures as a new tool of archaeological prospection to be combined with the usual geophysical investigations [1–11].

Optical multispectral sensors, such as Landsat TM and MSS, SPOT XI, and Terra ASTER, have been exploited within

* Corresponding author. Tel.: +39 06 4993 4479; fax: +39 06 4993 4211.
*E-mail addresses:* rosa.cavalli@lara.rm.cnr.it (R.M. Cavalli), francesca.colosi@itabc.cnr.it (F. Colosi), palombo@imaa.cnr.it (A. Palombo), pignatti@imaa.cnr.it (S. Pignatti), maurizio.poscolieri@idac.rm.cnr.it (M. Poscolieri).
[1] Tel.: +39 06 9067 2361; fax: +39 06 9067 2373.
[2] Fax: +39 0971 427271.
[3] Tel.: +39 06 4993 4110; fax: +39 06 2066 0061.

1296-2074/$ - see front matter © 2007 Elsevier Masson SAS. All rights reserved.
doi:10.1016/j.culher.2007.03.003

different archaeological contexts to highlight buried structures of historical significance in many environments [1–11]. In particular, Fowler [5] reports some applications of satellite images for archaeological prospection in the USA and the UK, speculating about their additional value compared to conventional aerial photographs. Fowler [5] and Aminzadeh and Samani [12], however, stress the lack of details in terms of archaeological results, due to insufficient spatial and spectral satellite resolutions. In addition, some archaeological applications of airborne multispectral R.S. data [13] indicate that, in general, Red, Near-infrared (N.I.R.), Short-wave infrared (S.W.I.R.) and Thermal-infrared (T.I.R.) regions can be exploited for buried structure detection. Following the hints of the above-mentioned works, it appears clear that remote, medium- or high-resolution spectral data can have new perspectives of application in archaeology or for the evaluation of environmental hazards.

The major drawback of insufficient spatial and spectral resolutions of R.S. data was overcome over the past decade with the advent of the high-resolution hyperspectral imaging scanners that can sample the electromagnetic spectrum with narrow consecutive spectral bands. Among the sensors operated on aerial platforms, noteworthy are the AHS, AHI, AVIRIS, CASI, and HYMAP. A few imaging spectrometer applications in cultural heritage frameworks are mentioned in the literature. In particular, Buck et al. [14] present the results of the sub-pixel capability of detecting obsidian and pottery artefacts scattered on the bare soil surface of a site in Western USA; visible and spectral bands were used. In contrast, Barnes [15] demonstrates the benefits of the combined use of LIDAR sensor and CASI images for identifying archaeological earthworks in southern England.

It appears evident, therefore, that it is of extreme interest to study the application of such new technologies in the framework of archaeological investigation. This is because the synoptic by-products of the hyperspectral image processing can be extremely effective when applied to those areas where large cultural heritage assets from ancient communities were to be discovered, surveyed, safeguarded from grave-robbers and protected from environmental degradation, mostly related to unchecked urban development. In this respect, the Italian peninsula contains a large number of ancient buried ruins consisting of either large centres (including entire urban structures) or buildings and town-walls which have to be still fully studied and excavated.

Within this context, this paper presents the results of the analysis of R.S. data collected over the Archaeological Park of Selinunte (SW Sicily, Italy) with the airborne Multispectral Infrared and Visible Imaging Spectrometer (M.I.V.I.S., Daedalus AA5000 [16]).

The paper addresses in Section 2 the issue of exploiting airborne hyperspectral imagery as a tool for archaeological prospection by defining two parameters which assess the hyperspectral R.S. aptitude to detecting anomalies related to buried structures. Section 3 describes the test area of Selinunte's Archaeological Park, while Section 4 deals with the M.I.V.I.S. hyperspectral data set and how the images were calibrated and corrected. The introduced indexes were applied (Section 5) to every M.I.V.I.S. single channel, to the outputs of selected processing methods (i.e. Principal Component Analysis and Apparent Thermal Inertial calculation) and to the by-products of supervised classification procedures (i.e. Spectral Angle Mapper and Minimum Distance). Moreover, in Section 5 the indexes are analysed with scatterplots. Section 6 presents the discussion of the obtained results, while the conclusions and implications are reported in Section 7.

## 2. Anomaly evaluation criteria

The identification of relevant archaeological marks, i.e. the tonal anomalies on the images, is mainly the result of the subjective experience of the photo-interpreter and of the knowledge of the context to which the images refer. For this reason, the use of R.S. in archaeology is still considered to be simply a descriptive discipline not supported by the analysis of statistical variables or quantitative indexes. In the attempt of recovering this gap, two parameters were defined to combine the subjective experience of the photo-interpreter with physical variables related to the spectral properties of the surface materials. The parameters show the potential of mark detection on the images, marks that give a hint of the presence of buried objects with an archaeological meaning: they take into account the amount of pixels pertaining to the corresponding anomalies and their brightness.

The first parameter, the *Detection Index* (D.I.), provides a quantitative measure of photo-interpretation analysis done on the images. D.I. is expressed by the following relation:

$$\text{D.I.} = \frac{Npixel_{\text{archa}}}{Npixel_{t-\text{archa}}} \times 100 \tag{1}$$

where, for a given area, $Npixel_{\text{archa}}$ is the number of pixels belonging to the archaeological marks in the interpreted image, while $Npixel_{\text{t-archa}}$ corresponds to the total number of pixels recognized as archaeological marks in the whole set of analysed images.

In contrast, the *Separation Index* (S.I.), gives an indication of the tonal difference between archaeological marks and background. The index is expressed as follows:

$$\text{S.I.} = \left(1 - \frac{\int D_{\text{archa}} D_{\text{bck}} \mathrm{d}x}{\sqrt{\int D_{\text{archa}}^2 \mathrm{d}x \int D_{\text{bck}}^2 dx}}\right) \times 100 \tag{2}$$

where $D_{\text{archa}}$ represents the frequency distribution of the digital values of the pixels belonging to the archaeological marks ($Npixel_{\text{archa}}$), while $D_{\text{bck}}$ represents the frequency distribution of the pixels selected as background. S.I. is, therefore, an indicator of the overlapping area of the two frequency distributions $D_{\text{archa}}$ and $D_{\text{bck}}$.

Fig. 1 shows the sequence of operations leading to the calculation of the S.I. value on a selected area. In particular, Fig. 1a depicts one of the interpreted images, where tonal

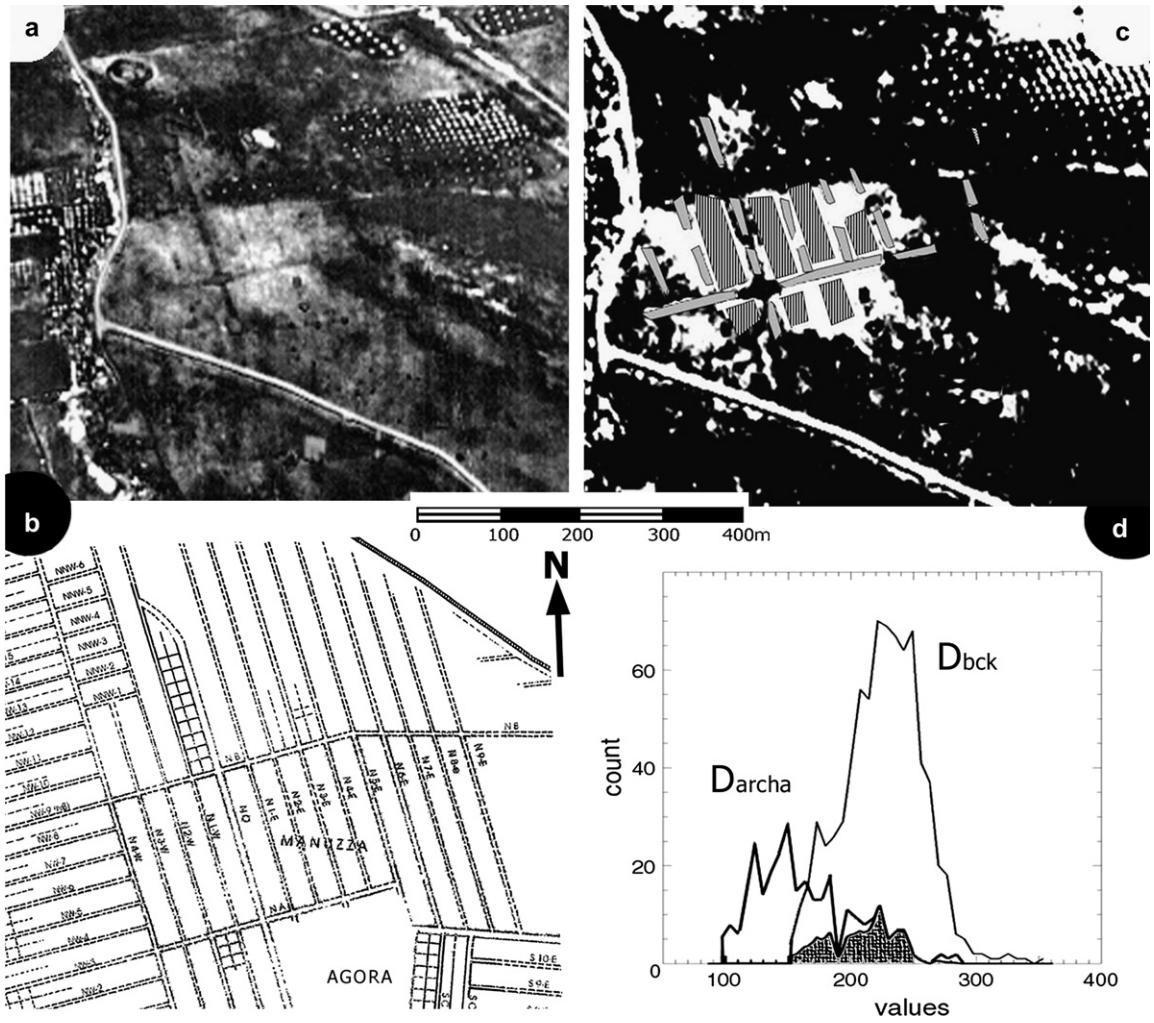


Fig. 1. (a) Subset of one interpreted M.I.V.I.S. image. (b) Archaeological sketch map [17]. (c) Arbitrarily stretched version of Fig. 1a with superimposed polygons referring to background (filled with vertical lines) and to archaeological lineaments (grey-shaded). (d) Frequency distributions of the anomaly pixels ($D_{archa}$) and of the background pixels ($D_{bck}$); the convolution product of the two distributions, represented by S.I., is shown with halftone grating.

lineaments are clearly visible and correspond to archaeological features as portrayed in the sketched map (Fig. 1b), drawn by archaeologists [17]. Fig. 1c shows the mask corresponding to the pixels (grey shaded) used for determining $D_{archa}$ and the mask (black polygon with vertical lines in Fig. 1c) pointing the background pixels describing $D_{bck}$. The plot of the two frequency distributions of archaeological marks and background pixels and their convolution product are reported in Fig. 1d.

As these indexes are normalized to the selected area, they can be applied to R.S. data regardless of the land cover scenario, the sensor data characteristics and the applied image processing techniques; consequently, they can be analysed and compared with one another. A significant test of the index efficiency can be performed by using hyperspectral data, because they can assume a wide dynamic range pointing out trends useful to stress the image most valuable in terms of anomaly detection. Since an image with the best possible sub-superficial structure prediction (i.e. high number of reliable marks) would determine a cluster of values in the upper right corner of the S.I. vs. D.I. space, this space can be used to rank the image ability of detecting anomalies.

## 3. The test area

The archaeological Park of Selinunte, located along the SW coast of Sicily (Fig. 2) and covering an area of about 2.5 km$^2$, is one of the outstanding cultural heritage sites of Southern Italy. It is spread over three N–S elongated hills, which exhibit the major axis orthogonal to the coastline: moving eastwards, they are the Gaggera, Manuzza and Eastern hills.

The city was founded in the 7th century BC by colonizers who came from Megara Hyblaea. The *Acropolis* (public and religious centre of the ancient cities) was located on a hilly area south of Manuzza Hill. During the two centuries that followed, the city spread eastwards and westwards, along the Cottone and Modione stream valleys, which stretch along the borders of Manuzza Hill and create two natural harbours at their confluence with the sea.

The ruins of the Acropolis area reveal a typical street network (Fig. 3) represented by a primary road, *Plateia,* running along the major axis of the hill, and a series of parallel secondary street axes termed *Stenophoi*, crossing the Plateia regularly at right angles. The Plateiae are as wide as ∼6 m,

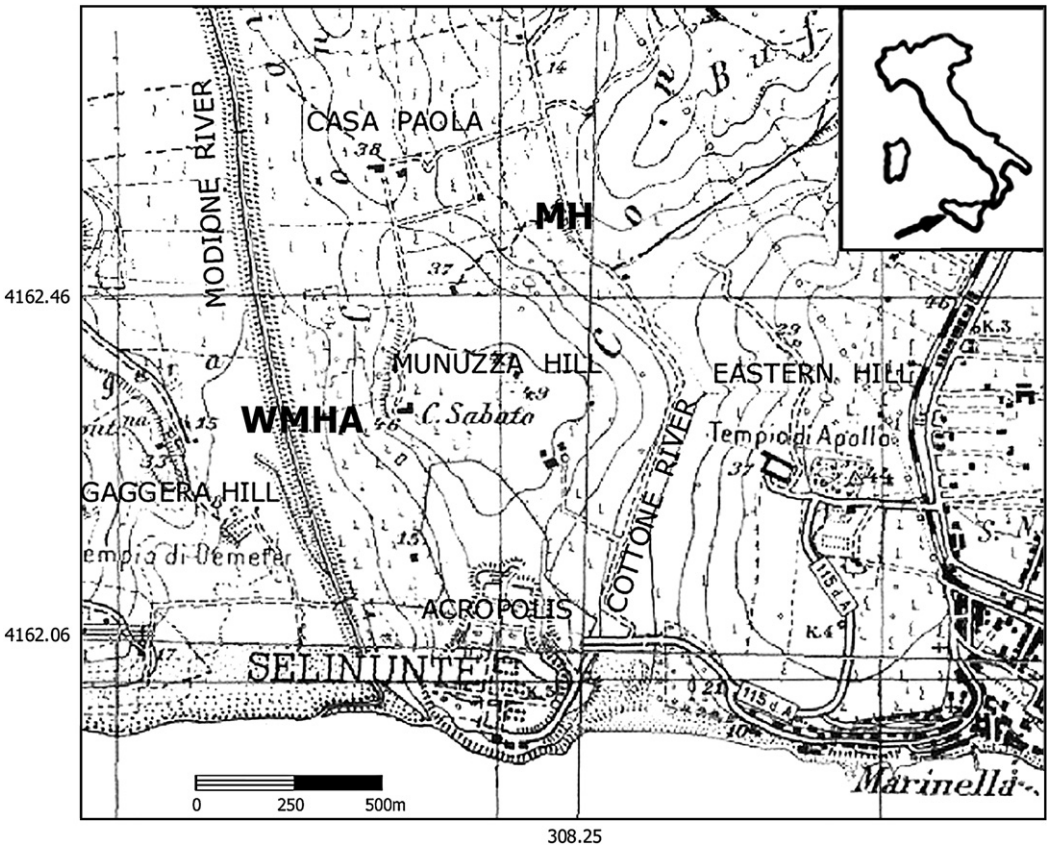


Fig. 2. Topographic map of the Selinunte Archaeological Park. MH and WMHA point out the two test areas. The study area is indicated on the top right.

whereas Stenophoi are, at maximum, 3 m wide; both are usually situated at a depth of about 50 cm below the ground. On the Gaggera and Eastern hills two religious areas were present, that were connected to the Acropolis area by a Plateia crossing the city area and passing through the urban defence walls.

Manuzza Hill exhibits a regular street pattern [18] tilted by 23° westwards with respect to that of the Acropolis area (Fig. 3); this network was first identified on aerophotos by Schmiedt [19] and partly confirmed by successive archaeological investigations [20,21] and by geomagnetic and geoelectric prospections [17]. Moreover, the town was surrounded by a huge town-wall system, the traces of which were studied by Mertens [17,22] and partially excavated.

The Selinunte area was selected for the present investigation because of the sharp geometry of the urban street network, already identified by means of historical aerophotos, geophysical surveys and excavation campaigns. Therefore, it represented an optimal test benchmark for studying the detection potential offered by hyperspectral M.I.V.I.S. data.

The D.I. and S.I. values were calculated in the Selinunte test area within two sectors, which exhibit uniform land covers and lithological outcrops, and where a statistically significant number of anomaly pixels were detected.

Such areas, shown in Figs. 2 and 3, correspond to:

- Manuzza Hill (hereafter referred to as M.H.);
- the western slope of Manuzza Hill and of the Acropolis area (hereafter referred to as W.M.H.A.).

At the time of the M.I.V.I.S. flight, the terrain cover consisted of spontaneous vegetation (grass and xerithic shrubs) characterized by different spatial density. The soil on M.H. was a weathering product of the underlying calcarenite formation covered by vegetation, while on W.M.H.A. the soil was interbedded with a clay–silt mixture with scarce vegetation cover.

### 3.1. Geology and land cover

During the Pliocene and Lower Pleistocene periods, the Selinunte area underwent a subsidence process, followed by extensional tectonics forming a graben, which determined the present-day morphological setting with three hills ending with small cliffs to the sea [23].

From a lithological point of view (see the description by Amadori [23]), the tops of the hills exhibit a bio-calcarenitic unit, cropping out with different levels of porosity and coherence, at times weathered and fractured. Along the hill slopes, a seldom cemented clayey sand occurs, with calcareous concretions locally interbedded with poorly cemented ochre calcarenitic lenses, while, moving downward, clays and clayey marls are present, dating back to the Lower Pleistocene. The valley bottoms are characterized by recent alluvial deposits, often exploited for agricultural purposes. In addition, sand dunes lie to the west of the Acropolis area and along its eastern slope, while clayey-sand layers are observed in the archaeological area where the detritus cover is thinner.

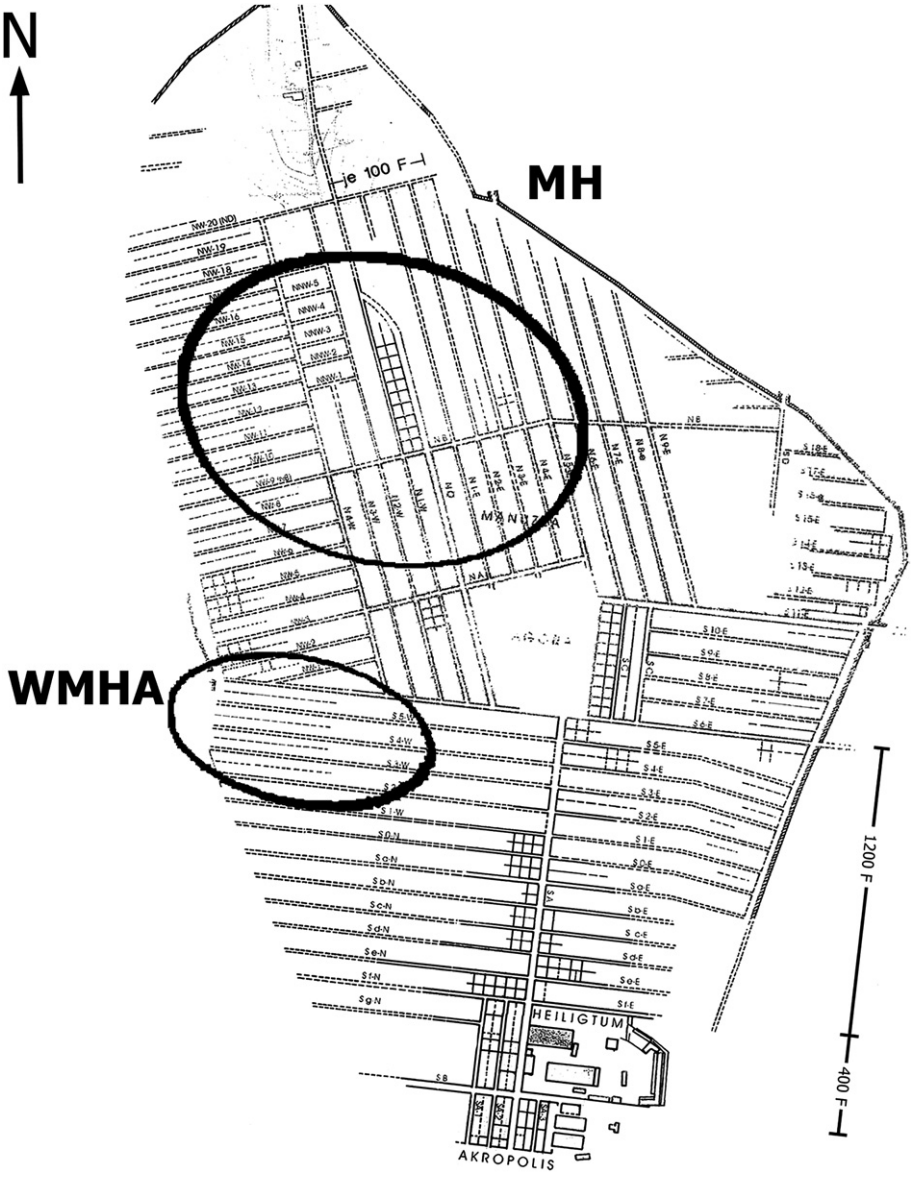


Fig. 3. The urban street pattern reconstruction performed by D. Mertens [17]. The two elliptical figures frame the two areas of investigation.

The land cover is composed mainly of natural vegetation, such as Mediterranean maquis along the coast line and the Modione creek valley, eucalyptus trees along the rural roads, xerithic shrubs and meadows near the ruins. The agricultural fields are characterized by olive-trees (mainly on the Eastern Hill), vineyards (along the western slopes of Manuzza Hill) and wheat in the north-eastern part of the study area.

## 4. M.I.V.I.S. sensor and data pre-processing

The M.I.V.I.S. spectrometer is an airborne passive remote sensing scanner [16] which records with an Istantaneous Field of View (I.F.O.V.) of 2 mrad the incoming radiation into four optical ports (see Table 1) covering the Visible (VIS), N.I.R., S.W.I.R. and T.I.R. spectral regions with 102 channels.

The remote survey over the Selinunte Archaeological Park was performed by the National Research Council, Airborne Laboratory for Environmental Research (L.A.R.A.) on May 23, 1996, at 12.30 h local time with clear sky conditions, from an altitude of 1500 m a.s.l. (3 m/pixel ground resolution).

The M.I.V.I.S. data were calibrated to instrument perceived radiances, using the internal reference sources and the calibration data gathered from the test bench. To remove the solar irradiance, atmospheric absorption and scattering effects that

Table 1
M.I.V.I.S. spectral characteristics

| Spectrometer # | Spectral region | No. of bands | Lower edge μm | Upper edge μm | Bandwidth μm |
|---|---|---|---|---|---|
| 1 | VIS | 20 | 0.43 | 0.83 | 0.020 |
| 2 | NIR | 8 | 1.15 | 1.55 | 0.050 |
| 3 | SWIR | 64 | 1.98 | 2.45 | 0.009 |
| 4 | TIR | 10 | 8.18 | 12.70 | 0.34 ÷ 0.54 |

can disturb (in terms of minor image contrast) the photo-interpretation process of the images, the bands of the first three spectrometers were converted to apparent reflectance by applying the ATmosphere REMoval Program (AT. REM. [24]) customized for the M.I.V.I.S. sensor [25]. Reflectance data were further cleaned of residual atmospheric effects by using EFFORT polishing techniques, as implemented in the ENVI software [26] by using also the spectra acquired on the field with the ASD FieldSpec Pro FR (350 to 2500 nm spectral range).

In contrast, the instrument perceived radiance values of the T.I.R. M.I.V.I.S. port were processed for obtaining the upwelling radiance at surface by tuning the M.I.V.I.S. thermal response to the TIMSCAL2 routine, implemented in the VICAR image processing software package, developed by NASA-JPL (http://www.openchannelfoundation.org). The kinetic temperature was then evaluated for all the T.I.R. M.I.V.I.S. channels by assuming a constant spectral emissivity value of 0.95.

## 5. Data analysis

In order to identify the spectral regions and processing techniques providing comparatively more archaeological information, hyperspectral M.I.V.I.S. data were analysed by using two separate processing approaches.

The first approach took into account the analysis of single channels, while a second one considered images resulting from combination of groups of spectral bands (Principal Components and Apparent Thermal Inertia) and of supervised classification procedures, such as Spectral Angle Mapper (S.A.M) and Minimum Distance (M.D.). The second approach was based on the hypothesis that the application of image analysis techniques to the entire M.I.V.I.S. data set could enhance, in the resulting images, the potential of anomalies detection with respect to each single band. Therefore, this method, reducing the number of images to be visually interpreted, could provide a comparatively more robust and quicker prospecting technique to support archaeological investigations.

In order to standardize the visual interpretation process, each image was treated by applying no spatial filters and contrast enhancement techniques. Moreover, a single operator interpreted all the images for reducing the uncertainties introduced by different photo-interpretation keys; furthermore, any extracted anomalies were then evaluated by an expert in order to determine their archaeological relevance.

### 5.1. Analysis of single images

All the 102 original M.I.V.I.S. bands were visually interpreted and the corresponding D.I. and S.I. values were calculated. The analysis of their respective scatterplot, as shown in Fig. 4, pointed out that the M.H. and W.M.H.A. areas exhibit different trends. In the W.M.H.A. area (bottom graph of Fig. 4) the S.I. value distribution appears, indeed, comparatively more spread than that of the M.H. area (see top of Fig. 4), which can be correlated with the different characteristics of the land cover and the different size of the buried structures.

In the M.H. area (top plot of Fig. 4) the highest values of both indexes are relative to the bands pertinent to the Visible Near Infrared (V.N.I.R.) region and, in particular, to the spectral range between 0.720 and 0.820 μm. Since these spectral bands are correlated with the peculiar spectral features of vegetation, they stress that the buried structures have a relevant effect on the V.N.I.R. spectral behaviour of the natural vegetation coverage.

In contrast, the bottom plot, concerned with the W.M.H.A. area, displays the highest index values in correspondence of the bands pertaining to the N.I.R., S.W.I.R. and T.I.R. regions: among them, the spectrum ranges from 1.425 to 1.525 μm, from 1.990 to 2.20 μm and from 8.785 to 9.600 μm appear particularly archaeologically significant. This larger number of noteworthy spectral regions, distributed along all of the spectrum with respect to the one highlighted in the M.H. zone, appears related to the major occurrence of soil coverage, whose spectral signature does not exhibit features sensitive to the presence of buried structures.

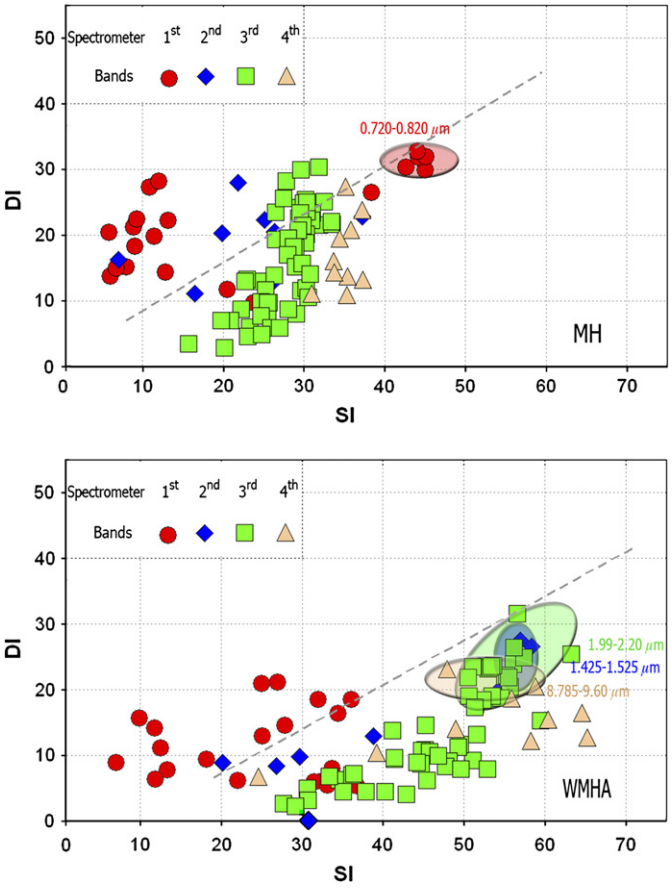


Fig. 4. The two scatterplots show the D.I. vs. S.I. computed from each single M.I.V.I.S. band for the M.H., W.M.H.A. areas. Bands are shown with different symbols and colour (see legend) according to their optical port (see Table 1). The highest values of D.I., S.I. are highlighted with ellipses and with the relative spectral ranges. The dashed line, drawn as reference, corresponds to the best fit of all interpreted images.

### 5.2. Analysis of multi-band images

Different processing techniques were applied to the hyperspectral data set to envisage which methodology better highlights anomalies generated by the change in the surface spectral properties induced by presence of buried structures. For this purpose, the results of the linear transformation of the N-band space (Principal Component Analysis) and of the combination of the thermal and visible part of the spectrum (Apparent Thermal Inertia) were compared, in terms of abundance and tonal intensity (i.e. D.I. and S.I. values) of the archaeological marks, with the outputs of the supervised classification procedures (Minimum Distance and Spectral Angle Mapper). This analysis is focused on the identification of a reduced number of output pictures which allows an easier and quicker visual interpretation.

#### 5.2.1. Principal Component Analysis

Principal Component Analysis (P.C.A.) was applied to the M.I.V.I.S. data for generating uncorrelated output bands, capable of better enhancing the tonal lineaments related to archaeological features. P.C.A. involves that the largest proportion of the data set variability, in the new orthogonal space, is concentrated in a few bands, called principal components (P.C.). The relative contribution of every original spectral band to a P.C. is then represented by the band's loading factor in the corresponding eigenvector of the covariance matrix.

Four P.C.A. runs, based on the covariance matrix calculation, were performed on M.I.V.I.S. subsets partitioned according to the four spectrometers wavelength ranges (see Table 1) in order to preserve the spectrum continuity.

Following the aforementioned visual interpretation criteria, the P.C. images were analysed in order to determine the corresponding D.I. and S.I. values. Their distribution is depicted in Fig. 5 for both the M.H. and W.M.H.A. areas, together with the mean index values ($\pm 1\sigma$ error bar) calculated over all the single bands belonging to every spectrometer, as shown in Fig. 4.

The relevance of the P.C. is mainly related to the remarkable increase in brightness of the tonal anomalies (i.e. S.I.) with respect to the analysis of the corresponding single image. Therefore, fewer images (P.C. bands) can be interpreted to obtain an amount of archaeological information (D.I.) which is a little larger compared to that obtained by the single image analysis. The higher S.I. values of the P.C. bands make the detection of the archaeological features easier and less affected by interpretation errors. Regarding the spectral ranges showing the best potential of anomaly detection, the indexes point out the same regions highlighted by analysing each M.I.V.I.S. band.

With regard to the archaeological interpretation of the structures detected by using the P.C.A. approach, the P.C.A. permitted the recognition of 13 well-defined NNW-SSE trending lines on the M.H. area and two others perpendicular to them, while, in the area located north of M.H., a distinct segment of the main street pattern and two orthogonal streets were detected. On the W.M.H.A. area, 4 small segments of linear features were discerned.

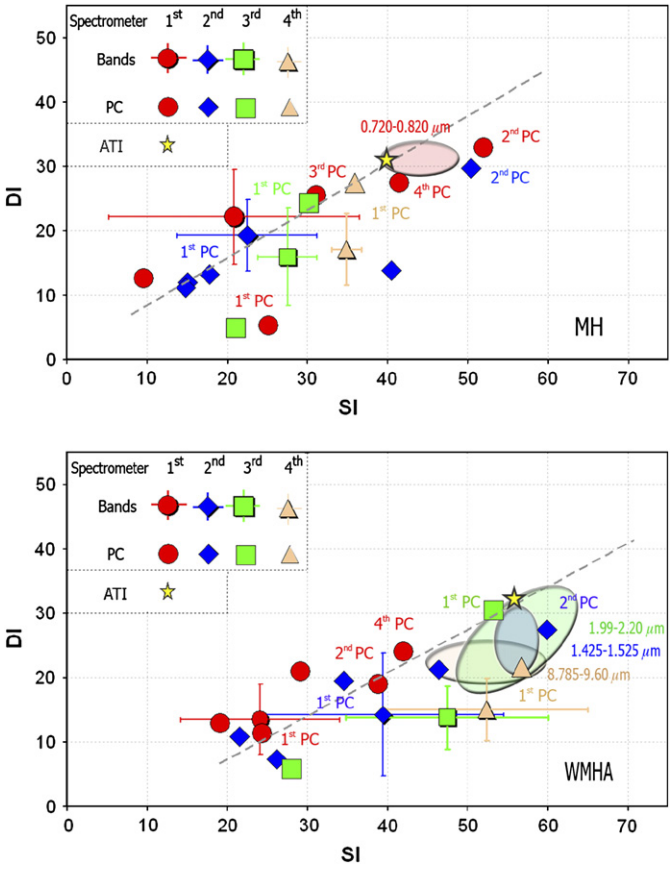


Fig. 5. The two scatterplots show the D.I. vs. S.I. calculated for the PC images (from 1st to 4th) and A.T.I. for the M.H., W.M.H.A. areas. The PC images are drawn with different symbols and colours (see legend) according to the optical port (see Table 1). The mean index values calculated over all the single bands of each spectrometer is also shown with the $\pm 1\sigma$ error bar. The ellipses and the dash line (the best fit of all interpreted images), as drawn in Fig. 4, are superimposed on the plots.

#### 5.2.2. Apparent Thermal Inertia

Apparent Thermal Inertia (A.T.I.) is a parameter well known by geologists and archaeologists [27,28] useful for the sub-superficial soil prospection. A.T.I. is a physical quantity related to thermal conductivity, density and thermal capacity and, therefore, it is sensitive to change in porosity and, subsequently, to the content of soil moisture [29]. A.T.I. is defined as the ratio, within a given time range, between the energy absorbed by surface materials and the corresponding temperature changes. A.T.I. is computed according to the following formula:

$$\text{A.T.I.} = (1 - A)/(T1 - T2) \quad (3)$$

where $A$ is the mean albedo computed by averaging the M.I.V.I.S. reflectance values from band 1 (0.44 μm) through band 13 (0.68 μm), and $T1$ represents daytime temperature derived by averaging the values of all M.I.V.I.S. thermal bands. $T2$, which usually indicates night-time temperature,

due to the lack of a pre-dawn M.I.V.I.S. overpass, was simulated by following the assumption described in Tonelli [30] that defined $T2$ with the following formula:

$$T2 = T_{\min} - 0.1(T1 - T_{\min}) \quad (4)$$

where $T_{\min}$ represents the lowest temperature in the image. This is surely a very robust assumption, but does not require the co-registration of the daytime and night-time temperature images with an accuracy at one-quarter of the pixel necessary to assure the perfect overlapping of the images.

A.T.I. exhibits values for the indexes greater than the corresponding values pertinent to the first P.C. calculated from the T.I.R. region (see Fig. 5), but lower in S.I. values, with respect to the corresponding values of the second PC bands derived from the V.N.I.R. and N.I.R. regions. This denotes that, with respect to the analysis of the T.I.R. single images and of the relative PCs, the combination of VIS and T.I.R. bands for calculating the ATI improves the D.I. (number of detected archaeological structures) and slightly the brightness contrast between anomalies and background (S.I.). This scenario is more evident in the W.M.H.A. area where soil cover is dominant.

The archaeological interpretation of ATI identified 9 of the aforementioned NNW–SSE trending lines in the M.H. area and 4 well-defined segments in the W.M.H.A. sector.

*5.2.3. Supervised classification approach*

Since the buried elements cannot be described by spectral signatures identified through either spectral endmembers or *regions of interest* (R.O.I.) on the image, it is not possible to derive a thematic map where these elements are univocally identified. Nevertheless, as the application of R.S. to archaeology is based on the assumption that sub-superficial structures generate slight differences in the spectral characteristics of the overlying terrains, distance based classification algorithms can be worthwhile for highlighting these spectral variations. This was tested by using the Spectral Angle Mapper (S.A.M.) [31,32] and the M.D. classification algorithms both based on the "spectral distance" criterion. The output of both classification methods was a thematic map and as many *Rule Images* (R.I.) as the input spectral classes. The thematic map is a parametric image where each pixel is characterized by a code, which is indicative of the class with the minimum distance from the pixel itself. The R.I., instead, returns the spectral distance value of the considered pixel with respect to each spectral class. As a consequence, the R.I.s for each pixel should be more sensitive to even small spectral variations related to changes of the surface physical/chemical characteristics than the output images of the aforementioned processing techniques.

The classification procedures were applied to 83 M.I.V.I.S. bands covering the first two and the third spectrometers up to 2.4 μm (thus encompassing the V.N.I.R. and S.W.I.R. spectral regions). Ten R.O.I.s representative of the main land cover units in the scene, were extracted directly on the screen by displaying False Colour Composites of M.I.V.I.S. bands and taking into account the information collected during the field surveys carried out for land cover check. The R.O.I.s were grouped into four main surface units:

- *Archaeological remains*, mainly consisting of calcarenite stones lying within the temple areas in the Acropolis area and on the Eastern hill (see Fig. 2);
- *Lithological outcrops* (partly mapped by Amadori [23], and checked during the field surveys), such as calcarenite, clay, sand, weathered calcarenite soil and calcarenite gravel making up the countryside road pavement;
- *Vegetation cover*, such as photosynthetic vegetation, dry shrubs, dry grass;
- *Water bodies*.

With regard to the Lithological Outcrops, the R.O.I.s were also defined by applying the Purity Pixel procedure (as implemented by ENVI software v4.0) for highlighting the purest endmember. The thematic maps resulting from the S.A.M. and M.D. classification techniques exhibit a good level of accuracy in terms of spatial distribution of the surface units, in agreement with the geologic map [23] and with field survey results, thus validating the selection of the input spectral classes as representative of the main land cover units.

*5.2.3.1. S.A.M. classifier.* According to the S.A.M. classification procedure, the R.I. pixel values represent, within the band space, the angular differences (expressed in radiance from 0 to $\pi/2$) between the spectrum of every pixel and the spectrum of one endmember. The algorithm determines the spectral similarity on the basis of the spectral shape and, thus, it is not sensitive to brightness differences. Therefore, the S.A.M. does not discriminate among different moisture content within the same terrain, which in the literature is reported as a primary factor for identifying buried structures [33].

The indexes calculated in the M.H. and W.M.H.A. areas, show (see Fig. 6) that the R.I.s of the S.A.M. exhibit the largest number of archaeological marks (D.I.) identified with the greatest brightness contrast between traces and background (S.I.). In the S.I. vs. D.I. space these index values appear clearly clustered in the upper right part of the scatterplots (markedly parted from the more scattered values relative to all the other methods), except for the indexes relative to the R.I. of dry grass. This result stresses that independently of the different soil coverage of the two test areas, the S.A.M. algorithm leads to the most relevant results in terms of archaeological detection performance.

The archaeological interpretation followed out in M.H. the 13 NNW–SSE trending segments of the ancient street network of the town and one segment orthogonal to them, stretching along the entire longitudinal axis of the hill. The two longest lineaments, with NNW–SSE orientation, continue as far as the Acropolis area, while in the W.M.H.A. area 5 linear structures were detected with E–W orientation.

*5.2.3.2. M.D. classifier.* As far as the M.D. classification algorithm is concerned, the relative pixel values of the R.I.

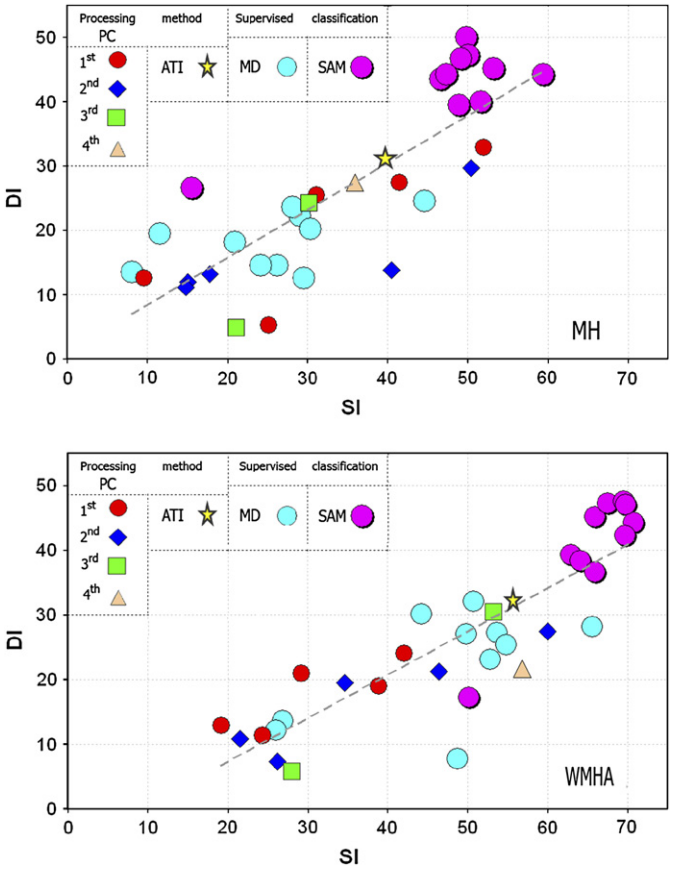


Fig. 6. The two scatterplots show the D.I. vs. S.I. values computed from the outputs of the processing method (P.C., A.T.I.) and the supervised classification (M.D., S.A.M.) for the M.H., W.M.H.A. areas. The P.C. bands are depicted with symbols and colours relative to M.I.V.I.S spectrometers (see legend). The dashed line corresponds to the best fit of these images.

are the Euclidean distance calculated between the spectrum of a pixel and the mean spectrum of every training spectral class. The M.D. algorithm estimates the similarity between two spectra in terms of intensity; for instance, spectra of the same terrain are considered dissimilar if characterized by different moisture content which controls the pixel brightness [34].

In the S.I. vs. D.I. space the index values of the marks identified on the R.I.s within the M.H. area (see top plot of Fig. 6), lie within the ranges defined by the single image analysis as shown in Fig. 4 and with values lower than the indexes obtained by the P.C. and A.T.I. analysis. The indexes computed for W.M.H.A., instead, are noticeably higher than the corresponding indexes obtained by the analysis of single images, A.T.I. and P.C.s, and they are closer to the values obtained with the S.A.M. Such evidence was checked by calculating the distance between the barycentre of the cloud of the S.A.M. and the M.D. index values: for M.H., the distance between the two barycentres is 33 while for W.M.H.A. it is 25. Concerning the archaeological relevance of the spectral classes, the primary contribution to archaeological prospection in both areas (pointed by high values of both indexes) was related to the class of weathered calcarenite (see Fig. 6).

The archaeological interpretation of all the R.I.s of the M.D. classification recognized 9 lineaments of the street network with NNW–SSE orientation. and one axis orthogonal to them in M.H, while only 5 linear structures with E–W orientation were detected in W.M.H.A.

## 6. Discussion

The distribution of S.I. vs. D.I. (Figs. 4–6) points out that the ‘band combination analyses’ reveal a higher tonal contrast with respect to the ‘single image analysis’. The advantage of using ‘band combination analyses’ is mainly based on the possibility to gather the archaeological information content of the entire hyperspectral data set in a reduced number of images as a function of the soil cover typology (different behaviour for M.H. and W.M.H.A.).

The linear combination of the N-band spectral space in the P.C. transformation and in the A.T.I. product does not produce images with a noteworthy increase of the archaeological information content. This is expressed in terms of a similar number of marks (D.I.), even though it determines a slight increment of their contrast (S.I.), thus helping the interpreter’s work in drawing the marks. The plots of the single images (Fig. 4), the P.C. and the A.T.I. images reveal that their archaeological information content is comparable and it is related to the different land cover characteristics. These methods point out a similar spectral range as the most relevant in terms of archaeological information.

V.N.I.R. and specifically the 0.68–0.82 μm spectral range appears noteworthy where the natural vegetation is related to the absorption peak of red and the infrared plateau of vegetation. On the contrary, the N.I.R. (bands between 1.42 and 1.52 μm), S.W.I.R. (bands between 1.99 and 2.2 μm) and T.I.R. (channels between 8.785 and 9.60 μm) spectral ranges appear the most useful in terms of archaeological information where bare soil coverage becomes relevant. Spectrum of Selinunte bare soil, in fact, does not exhibit any peculiar peaks that change with the presence or absence of the buried structures.

An important increment in the ability of detecting marks (Fig. 6), instead, is attained by the application of image processing techniques such as the classification algorithms that improve the potential of anomaly detection related to man-made structures according to the goodness of the training class selection.

The plot of the index values (Fig. 6), calculated from all the band combination images (S.A.M., M.D., A.T.I., P.C.s), shows a clear direct linear correlation between the two indexes ($R^2 = 0.676$ for M.H. and $R^2 = 0.722$ for W.M.H.A.); this stresses that in those areas characterized by higher tonal differences it is possible to count more archaeological marks and vice versa. Since the regression line built for the W.M.H.A. area intersects the S.I. axis, this points out that in this area there is a threshold limit for the detection of the anomalies. This threshold, which is not present in the M.H. area, could be related to the different widths of the street axes buried in the two areas: M.H. exhibits both Plateiae, as wide as

~6 m, and Stenophoi, as wide as 3 m, whereas W.M.H.A. exhibits only Stenophoi. As a consequence, it can be derived that a different tonal intensity of the archaeological marks is required for detecting a comparable number of anomalies.

To assign an archaeological value to the marks detected on the hyperspectral data set, the tonal anomalies were evaluated by experts to verify their consistency with the state-of-art of archaeological information about the ancient Selinunte site. This analysis identified (Fig. 7) in M.H. 13 NNW–SSE trending street axes of the ancient town and two streets orthogonal to them. The longest among the 13 lineaments was associated to the Plateia 0 by Di Vita [18], and its parallel street to the West was identified as Stenophòs I West by Di Vita [18,21], the traces of which can be followed as far as the southern boundary of the hill. Curvilinear traces found along the northern slope of M.H. seem to correspond to town-wall remains. The same area shows one NNW–SSE trending lineament and 2 orthogonal traces that could testify a northward extension of the main street system of the city. This archaeological outcome was hypothesized by Zoppi [35] and confirmed by Mertens [17] on the basis of geophysical surveys. In the Cottone creek valley, to the east of the Acropolis area, two E–W trending lineaments were checked in 2003 by field geophysical surveys. Along the left bank of the Modione creek (W.M.H.A. area), some segments of 9 linear structures with E–W orientation were detected. This pattern, confirmed by excavation test sites [36–40]and by geophysical surveys [21], represents the extension of the Acropolis street system.

In order to evaluate how better these results are than those derivable by investigating historical aerophotos, a similar procedure was applied to the available frames. Such pictures were collected in 1968 on 1:13,500 scale, in 1971 on 1:4000 and 1:8000 scales, in 1973 on 1:5000 and 1:10,000 scales, in 1975 and in 1987 on 1:10,000 scale as colour prints, and in 1993 on 1:8000 scale. The aerial photos, taken in 1971, 1975 and 1993, identify traces that are mostly located in the M.H. area and correspond to the main street axes with NNW–SSE orientation. Among the analysed frames, the 1975 pictures proved to be helpful for detecting the street major axis *Plateia 0* [18] on M.H., the anomalies on the Eastern hill, probably related to a Roman villa, and some irregularly shaped traces along the northern slopes of M.H., also visible on the 1971 photos. As a whole, the analysed historical frames made it possible to depict in M.H. the main NNW–SSE trending street network, while the aerophotos interpreted by Schmiedt [19] allowed the identification of traces of the main network and two lineaments orthogonal to it.

This analysis has stressed that single M.I.V.I.S. bands carry archaeological information comparable to that derived by interpreting the available aerophotos, while best results, in terms of number of identified structures and anomaly tonal intensity, are obtained by analysing the output of M.I.V.I.S. data processing (Fig. 7).

These differences highlight the greater detection efficiency of a single hyperspectral survey, with respect to aerial photographs acquired in different years and under various environmental conditions (as was also surmised by Fowler [5]).

## 7. Concluding remarks

The proposed study has shown that airborne hyperspectral R.S. is a powerful prospection tool for identifying marks related to sub-superficial archaelogical structures. These structures yield variations in the spectral properties of terrain surfaces clearly perceptible on the hyperspectral images as tonal anomalies.

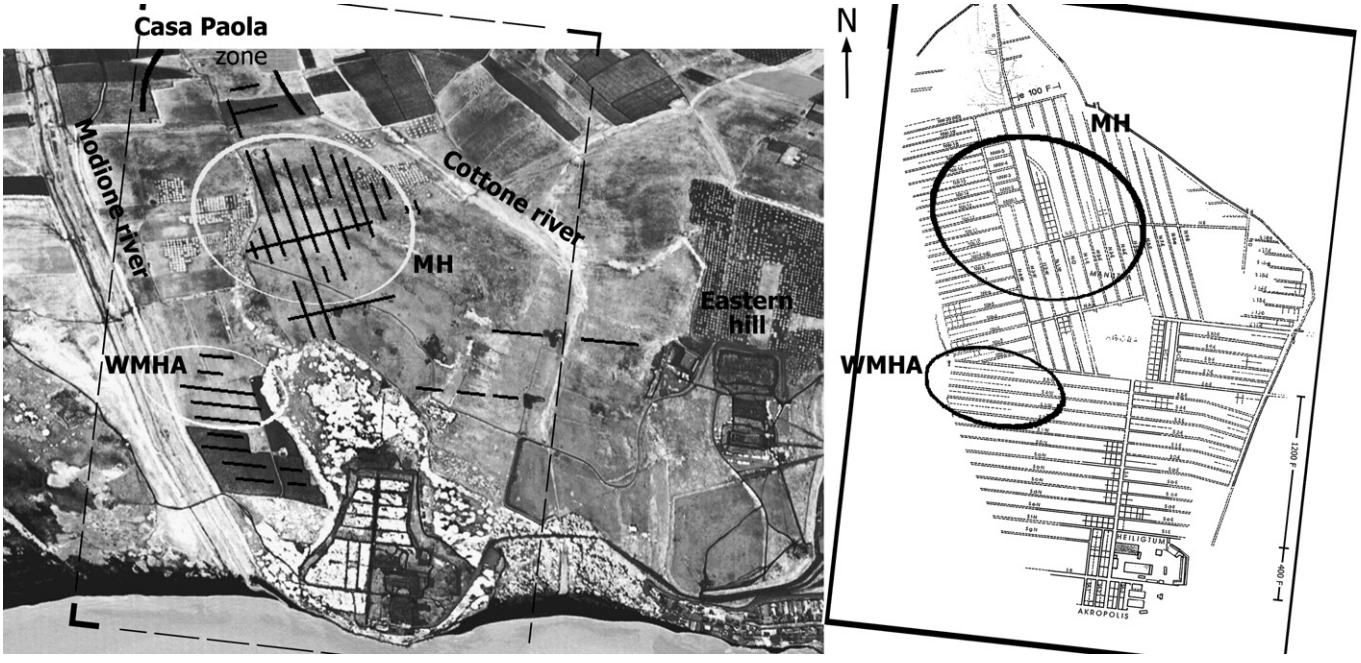


Fig. 7. The left picture shows the ensemble of the archaeological anomalies highlighted by all by-products of M.I.V.I.S. data; the right picture shows the street network highlighted by the geophysical surveys [17].

The image processing techniques applied to M.I.V.I.S. data provided the highest archaeological content and allowed to concentrate this content in a few images, making the image interpretation procedure quick and efficient in terms of archaeological detection. Moreover, the wide spectral range sampled by the hyperspectral scanner allowed determination of which spectral range is the most valuable to highlight anomalies.

The archaeological detection relevance of the airborne remotely sensed hyperspectral data was evaluated by introducing two new indexes, the Detection Index and Separability Index, which respectively describe the archaeological detection potential of an image in terms of amount and tonal intensity of the marks. The comparative analysis of the index values in the S.I. vs. D.I. space allowed ranking of the archaeological information content gathered by the interpreted images.

It was established that, where land cover is mainly characterized by spontaneous vegetation (i.e. grass and xeritic shrubs), the VIS-N.I.R. ranges appear the most significant spectral regions for the archaeological detection. Conversely, where the vegetation cover is sparse, tonal changes related to buried remains can also be perceived in the S.W.I.R. region, according to the soil local spectral characteristics, and in the T.I.R. region of the spectrum.

It was verified that the best performing processing method is the S.A.M. algorithm, based on the angular distance parameter, whose index values appear the most clustered in the S.I.–D.I. space and invariant with respect to the land cover. In particular, the S.A.M. algorithm is performing quite well in terrains with a large presence of vegetation because it allows measurement of the slight changes in vegetation status induced by sub-superficial structures, while it is not sensitive to the soil brightness variations. Similarly, in terrains with a larger occurrence of soil components, the M.D. algorithm, based on the Euclidean distance parameter, is sensitive to the soil brightness variations that can be correlated to changes in moisture content induced by buried structures.

Regarding the archaeological structures identified by analysing the M.I.V.I.S. data over the Selinunte test site, the results appear to match those of an extensive geophysical survey carried out throughout the area of the ancient city [17]. In particular, the presence of segments of town-walls and traces of the urban street network to the north of Manuzza Hill near Casa Paola was confirmed.

As final remark, the archaeological results gathered from the data processing flow chart applied to the M.I.V.I.S. data over Selinunte appear to be encouraging for prospecting archaeological structures. Therefore, such analysis is suitable for future applications in other areas with different land cover and anomaly characteristics, in order thus to confirm the aptitude of the hyperspectral data as a new complementary tool for archaeological prospection.

## 8. List of acronyms and abbreviations

A.T.I. apparent thermal inertia
AT. REM. ATmosphere REMoval
D.I. detection index
I.F.O.V. istantaneous field of view
L.A.R.A. Airborne Laboratory for Environmental Research
M.D. minimum distance algorithm
M.H. Manuzza Hill
M.I.V.I.S. multispectral infrared and visible imaging spectrometer
N.I.R. near infrared
P.C. principal components
P.C.A. principal component analysis
R.I. rule image
R.O.I. region of interest
R.S. remote sensing
S.A.M. spectral angle mapper algorithm
S.I. separability index
S.W.I.R. short wave infrared
T.I.R. thermal infrared
VIS visible
V.N.I.R. visible near infrared
W.M.H.A. western slope of Manuzza Hill and of the Acropolis

## Acknowledgements

The authors are grateful to S. Zoppi who granted this study. Moreover, they are grateful to V. Cuomo and G.P. Gregori for their scientific reviews of the paper.

## References

[1] I. Scollar, A. Tabbagh, A. Hesse, I. Herzog, Archaeological Prospecting and Remote Sensing, Cambridge University Press, 1990.
[2] I. Shennan, D.N.M. Donoghue, Remote sensing in archaeological research, In: Proceedings of the British Academy, 77, Oxford University Press, 1992, pp. 223–232.
[3] M.J.F. Fowler, Detection of archaeological features on satellite imagery, AARGnews 10 (1995) 7–14.
[4] M.J.F. Fowler, A high-resolution satellite image of archaeological features of the south of Stonehenge, International Journal Remote Sensing 22 (7) (2001) 1167–1171.
[5] M.J.F. Fowler, Satellite remote sensing and archaeology: a comparative study of satellite imagery of the environs of Figsbury Ring, Wiltshire, Archaeological Prospection 9 (2) (2002) 55–69.
[6] F. Colosi, L. Pompeo, M. Samgiorgio, C. Zamboni, Elaborazione ed interpretazione di immagini telerilevate per lo studio sistematico delle testimonianze antropiche nel territorio. I casi di Palmyra e Selinunte, Archeologia e Calcolatori 6 (1995) 35–60.
[7] N.A. Drake, Recent Aeolian origin of surficial gypsum crusts in southern Tunisia: Geomorphological, archaeological and remote sensing evidence, Earth Surface Processes and Landforms 22 (7) (1997) 641–656.
[8] A.M. Montufo, The use of satellite imagery and digital image processing in landscape archaeology. A case study from the island of Mallorca, Spain, Geoarchaeology 12 (1997) 71–85.
[9] R.G. Blom, B. Chapman, E. Podest, R. Murowchick, Application of remote sensing to archaeological studies of early shang civilzation in northern China, in: T.I. Stein (Ed.), Proceedings of the International Geoscience and Remote Sensing Symposium 2000, Honolulu, Hawaii, USA, 24–28 July 2000, 6, pp. 2483–2485.
[10] C.J. Colleman, M. Crawford, P. Lehman, G. Nikolaenco, J. Trelogan, The Chora of Chersonesos in Crimea, Ukraine, American Journal of Archaeology 104 (2000) 707–714.

[11] E. Ben-Dor, M. Kochavi, L. Vinizki, M. Shionim, J. Portugali, Detection of buried ancient walls using airborne thermal video radiometry, International Journal of Remote Sensing 22 (18) (2001) 3689–3702.
[12] B. Aminzadeh, F. Samani, Identifying the boundaries of the historical site of the Persepoli using remote sensing, Remote Sensing of Environment 102 (2006) 52–62.
[13] D. Powlesland, J. Lyall, D. Donoghue, Enhancing the record through remote sensing: the application and integration of multi-sensor, non-invasive remote sensing techniques for the enhancement of the sites and monuments record, In: Heslerton Parish Project, 2, Internet Archaeology, North Yorkshire, England, 1997.
[14] P.E. Buck, D.E. Sabol, R. Alan, A.R. Gillespie, Sub-pixel artefact detection using remote sensing, Journal of Archaeological Science 30 (2003) 973–989.
[15] I. Barnes, Aerial remote-sensing techniques used in the management of archaeological monuments on the British Army's Salisbury Plain Training Area, Wiltshire, UK, Archaeological prospection 10 (2) (2002) 83–90.
[16] R. Bianchi, C.M. Marino, S. Pignatti, Airborne hyperspectral remote sensing in Italy. Recent advances in remote sensing and hyperspectral remote sensing, in: Proceedings EUROPTO Series SPIE 2318, 27–29 September, Rome, Italy, 1994, pp. 29–37.
[17] D. Mertens, I. Selinus, Die Stadt und ihre Mauern, Verlag Philipp von Zaberm, Mainz am Rein, Germany, 2003.
[18] A. Di Vita, L'urbanistica della Sicilia greca, In: I greci in Occidente, Bompiani Publisher, Venice, Italy, 1996, 263–308.
[19] G. Schmiedt, Applicazioni della fotografia aerea in ricerche estensive di topografia antica in Sicilia, Kokalos 3 (1957) 18–30.
[20] A. Rallo, Scavi e ricerche nella città antica di Selinunte. Relazione preliminare, Kokalos 22/23 (1976–77) 720–723.
[21] A. Rallo, Nuovi aspetti dell'urbanistica selinuntina, ASAtene 46 (1984) 81–96.
[22] D. Mertens, Die Mauern von Selinunt, in: Vorbericht der Arbeiten des Deutschen Archeologischen Instituts Rom 1971–75 und 1985–87, Rome 96 (1989) 87–154.
[23] M.L. Amadori, M. Feroci, L. Versino, Geological outline of Selinunte Archaeological Park, Bollettino di Geofisica Teorica e Applicata 34 (134-135) (1992) 87–99.
[24] A.F.H. Goetz, J.W. Boardman, B. Kindel, K.B. Heidebrecht, Atmospheric corrections: On deriving surface reflectance from hyperspectral imagers, in: Proceedings SPIE Annual Meeting, 27 July 1997, San Diego, CA, USA, 3, 118, pp. 14–22.
[25] V. La Norte, S. Pignatti, V. Tramutoli, Extending the Use of Atrem Atmospheric correction to, M.I.V.I.S. data, in: Proceedings of SPIE, Remote Sensing for Environmental Monitoring, GIS Applications, and Geology, 18–21 September, Toulose, France, 4545, 2001, pp. 285–289.
[26] J.W. Boardman, Post-ATREM polishing of AVIRIS apparent reflectance data using EFFORT: a lesson in accuracy versus precision, in: Summaries of the Seventh JPL Airborne Earth Science Workshop, JPL Publication 97-21 (1) (1998) 53.
[27] A.B. Kahle, Surface emittance, temperature, and thermal inertia derived from Thermal Infrared Multispectral Scanner (TIMS) data for Death Valley, California, Geophysics 52 (7) (1987) 858–874.
[28] E. Ben-Dor, J. Portugali, M. Kochavi, M. Shimoni, L. Vinitzky, Airborne Thermal video radiometry and excavation planning at Tel Leviah, Golan Heights, Israel, Journal of Field Archaeology 26 (2) (1999) 117–127.
[29] R.P. Gupta, Interpretation of data in Thermal Infrared region, In: Remote Sensing Geology, Springer, Berlin, Germany, 1991, 125–146.
[30] A. Tonelli, Metodi di Telerilevamento da postazione fissa nella caratterizzazione di superfici e del primo spessore di massa, Rivista Italiana di Telerilevamento 1-2 (1995) 13–22.
[31] F.A. Kruse, A.B. Lefkof, J.W. Boardman, K.B. Heidebrecht, A.T. Shapiro, J.P. Barloon, A.F.H. Goetz, The spectral image processing system (SIPS)—Interactive visualization and analysis of imaging spectrometer data, Remote Sensing of Environment 44 (1993) 145–163.
[32] R.H. Yukas, A.F.H. Goetz, Comparison of airborne (AVIRIS) and spaceborne (TM) borne imagery data for discriminating among semi-arid landscape endmembers., in: Proceedings of the ERIM Ninth Thematic Conference on Geologic Remote Sensing, Ann Arbor, MI, USA, 8–11 February 1993, pp. 503–511.
[33] K.L. Kvamme, Terrestrial remote sensing in archaeology, in: H. Maschner, C. Chippindale (Eds.), Handbook of Archaeological Methods, AltaMira, 2005, pp. 1–23.
[34] L. Weidong, F. Baret, G. Xingfa, T. Qingxi, L. Zheng, B. Zhang, Relating soil surface moisture to reflectance, Remote Sensing of Environment 81 (2002) 238–246.
[35] C. Zoppi, Note Selinuntine, in: Monografia Selinunte, 3, Italy, Bulzoni, Rome, 1996, pp. 137–206.
[36] J. De La Genière, D. Theodorescu, Ricerche topografiche nell'area di Selinunte, RAL VIII, XXXIV (1979) 385–395.
[37] J. De La Genière, A propòs de deux sondages extramuros de l'acropole de Sélinonte, in: Philias Charin Miscellanea di studi classici in onore di, E. Manni, Roma 4, 1980, pp. 1293–1299.
[38] J. De La Genière, Nuove ricerche sulla topografia di Selinunte, RAL VIII XXXVI (1981) 211–217.
[39] J. De La Genière, Sélinonte. Recherches sur la topographie urbaine, ASNP III XII (1982) 471–479.
[40] J. De La Genière, J. Rougetet, Recherches sur la topographie de Sélinonte. Campagne 1985, RendLinc 40 (1986) 289–297.